This article is published as part of the *Dalton Transactions* themed issue entitled:

Dalton Transactions 40th Anniversary

Guest Editor Professor Chris Orvig, Editorial Board Chair
University of British Columbia, Canada

Published in issue 40, 2011 of *Dalton Transactions*

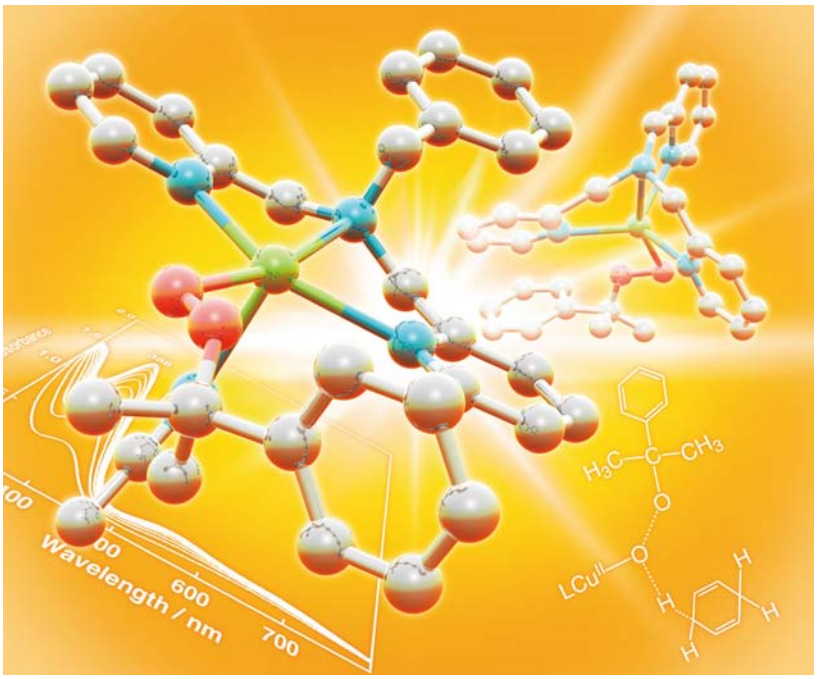

Image reproduced with permission of Shinobu Itoh

Welcome to issue 40 of the 40th volume of Dalton Transactions-40/40! Articles in the issue include:

PERSPECTIVE:

FRONTIER:

ARTICLES:

Visit the *Dalton Transactions* website for more cutting-edge inorganic and organometallic research
www.rsc.org/dalton

Dalton Transactions

Dynamic Article Links

Cite this: *Dalton Trans.*, 2011, **40**, 10708

www.rsc.org/dalton

PAPER

Experimental charge density study into C–C σ-interactions in a Binor-S rhodium complex†

Hazel A. Sparkes,*[a] Tobias Krämer,[b] Simon K. Brayshaw,[c] Jennifer C. Green,[b] Andrew S. Weller[b] and Judith A. K. Howard[a]

Received 22nd February 2011, Accepted 2nd August 2011
DOI: 10.1039/c1dt10303b

Transition-metal complexes containing (C–C)→M σ-interactions have potential applications in both catalysis and the activation and cleavage of C–C bonds. Fully characterising the bonding and interactions in complexes containing such (C–C)→M σ-interactions is vital to understand their chemical behaviour. As a result a high-resolution experimental X-ray charge density study has been undertaken on [Rh(Binor-S)(PCy_3)][$HCB_{11}Me_{11}$] (Binor-S = 1,2,4,5,6,8-dimetheno-*s*-indacene) which contains a (C–C)→Rh interaction. The data are analysed using Bader's "Atoms in Molecules" (AIM) approach with particular attention paid to the interactions around the rhodium centre. The results provide clear evidence for the σ(C–C)→Rh interaction in the solid-state which is classified as a weak covalent interaction. These results are supported by theoretical calculations.

Introduction

The coordination of transition-metal centres with saturated bonds (so–called σ-complexes), such as H–H, C–H and B–H, is of significant interest with regard to their central role in developing ideas in fundamental structure and bonding in transition-metal complexes and the activation and subsequent utilisation of element–element single bonds in chemical synthesis and catalysis.[1] Compared to dihydrogen[2] and C–H intermolecular agostic bonds,[3] metal···C–C σ-complexes are under-represented,[4,5] and their characterisation in the solid-state is a rare occurrence.[6,7] Intermediates in transition-metal promoted[8] C–C activation processes (oxidative cleavage) are often proposed to contain M···(C–C) σ-interactions.[9] As breaking strong C–C bonds tends to be thermodynamically and kinetically unfavourable, one approach to this is to use strained systems, such as cyclopropanes, where the reduction in strain in the system provides the driving force for the process.[4] We have recently reported the synthesis and solid-state structures of a set of complexes of formula [Rh(Binor-S)(PR_3)][$BAr^F{}_4$] [**1–R][BAr$^F{}_4$]** [R = iPr, Cy, Cyp; Binor-S = 1,2,4,5,6,8-dimetheno-*s*-indacene; Ar^F = $C_6H_3(CF_3)_2$].[7] These complexes have a formally Rh(III) {$Rh(PR_3)$}$^+$ fragment coordinated to a saturated organic ligand (Binor-S) through a metallacyclobutane ring and

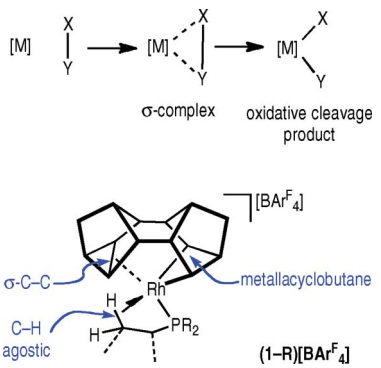

Fig. 1 (top) C–C activation *via* a σ-complex; (bottom) line diagram of BINOR-S complexes.

σ-C–C interaction from a cyclopropane unit (Fig. 1). There is also suggested to be a supporting, weak, C–H···Rh agostic interaction that completes the coordination sphere. The bonding in these molecules, and especially the σ-C–C interaction, has previously been characterised by X-ray crystallography, solution NMR data and computation. To complete the definitive characterisation of these unique molecules we now turn to an experimental charge density study.

Experimental X-ray charge density studies are challenging, particularly when heavy atoms are involved, however they can provide unique insights into the nature of bonding within a molecule as well as intermolecular interactions between the molecules under study. Such experiments require high-resolution X-ray diffraction data (2θ ~ 100°) to be collected carefully from good quality single crystals, followed by detailed analyses of the results of a multipole refinement. In order to characterise the bonds and interactions in the system under study, Bader's quantum

[a]*Department of Chemistry, University of Durham, South Road, Durham, DH1 3LE, UK. E-mail: h.a.sparkes@durham.ac.uk; Fax: (+) 44 191 334 2051*
[b]*Inorganic Chemistry Laboratories, University of Oxford, South Parks Road, Oxford, OX1 3QR, UK*
[c]*Department of Chemistry, University of Bath, Claverton Down, Bath, BA2 7AY, UK*

† Electronic supplementary information (ESI) available. CCDC reference number 814709. For ESI and crystallographic data in CIF or other electronic format see DOI: 10.1039/c1dt10303b

theory of Atoms in Molecules (AIM) is invaluable, chemical interactions are classified on the basis of the topological properties of the electron density [$\rho(\boldsymbol{r})$] and its Laplacian at [$\nabla^2\rho(\boldsymbol{r})$] at bond critical points (bcps) which are located along atomic interaction lines (AILs) or bond paths.[10] Shared shell covalent interactions have large positive values of $\rho(\boldsymbol{r})$ and negative values of $\nabla^2\rho(\boldsymbol{r})$, while positive values for both $\rho(\boldsymbol{r})$ and $\nabla^2\rho(\boldsymbol{r})$ are associated with closed shell ionic interactions.

A charge density study into a Ti-metallocyclobutane-based complex containing σ-C–C interactions has recently been reported.[11] The σ-interactions were identified in the titanacyclobutane fragment formed through the interaction of Ti with three carbon atoms of a neopentadiyl fragment. The interactions resulted in the electron density in the C–C bonds having an asymmetric shape with the distortion towards the metal centre most apparent on the C_α side of the C–C bcp. In addition, it was noted that the C–C bonds involved in the σ-interaction had small increases in their bond lengths (~0.03 Å) and significantly larger ellipticities when compared to other single C–C bonds in the structure. While experimental charge density study into σ-C–C interactions are rare, by comparison there are a relatively large number of reports on compounds containing agostic C–H bonds.[12]

Given that **[1–R][BAr$^F_4$]** represent well–characterised complexes with σ-C–C interactions, it is of particular interest to obtain experimental charge density measurements, as these would provide detailed, and complementary, insight into the bonding in these unique materials. However, the $[BAr^F_4]^-$ anion presents problems in charge density studies as the CF_3 groups are invariably disordered. One alternative is to use the anion $[HCB_{11}Me_{11}]^-$,[13] which can also support low-coordinate metals but tends not to be disordered, this anion has been used previously to partner low-coordinate silver(I) and zirconium cations.[14] In addition, the large size of the complexes, the presence of a second-row transition metal and the difficulties isolating good quality single crystals of such species makes this a challenging task. In view of this we have recently undertaken several charge density analyses on smaller precursors complexes $Rh(C_7H_8)(PR_3)Cl$ (R = PPh_3, P^tBu_3 and PCy_3),[15] which serve as benchmarks for the present analysis of $[Rh(C_{14}H_{16})(PCy_3)][HCB_{11}Me_{11}]$, **[1–Cy][HCB$_{11}Me_{11}$]**. Particular focus will be given to the nature of the interactions around the rhodium metal centre. These demonstrate that the Rh···σ-C–C interaction is indeed best described as being a weak covalent bond, in line with previously reported X-ray diffraction, NMR spectroscopy and computational analyses.

Results and discussion

$Rh(C_{14}H_{16})(PCy_3)][B_{11}C_{12}H_{34}]$, **[1–Cy][HCB$_{11}Me_{11}$]**, contains a formally 14-electron rhodium(III) cation consisting of tricyclohexylphosphine and the Binor-S fragment bound to the rhodium metal centre, as well as a carborane anion, see Fig. 2. A high-resolution low-temperature charge density dataset was collected up to $\sin\theta/\lambda = 1.06$ Å; two high-angle reflections were missing and the data collection and refinement details for **[1–Cy][HCB$_{11}$Me$_{11}$]** are summarised in Table 1. Although the focus of this investigation was to study the nature of the bonding around rhodium in the cation, by chance the anion is also of interest from a charge density perspective and so will also be discussed.

Table 1 Crystal data and structural refinement details for $[Rh(C_{14}H_{16})(PCy_3)][B_{11}C_{12}H_{34}]$, **[1–Cy][HCB$_{11}Me_{11}$]**

Empirical formula	$C_{44}H_{83}B_{11}PRh$
M_r	864.89
λ/Å	0.71073
Crystal system	Monoclinic
Space group	$P2_1/n$
a/Å	15.2225(1)
b/Å	13.2777(1)
c/Å	23.5072(1)
β (°)	102.521(1)
V/Å^3	4638.27(5)
Z	4
T/K	100(2)
D_c/Mg m^{-3}	1.239
μ/mm^{-1}	0.434
$F(000)$	1848
Crystal size/mm	0.20 × 0.22 × 0.24
θ range for data collection (°)	1.46 to 48.88
Ranges hkl	−32 to 32, −28 to 28, −49 to 49
Reflections collected	484435
Independent reflections	46189
$R_{int(merged)}$	0.0556
Spherical atom refinement	
No. data in refinement	46189
No. refined parameters	529
GOF (F^2)	1.045
Final R_1 [$I > 2\sigma(I)$] (all data)	0.0357 (0.0575)
wR_2 [$I > 2\sigma(I)$]	0.0764
$\Delta\rho_{max/min}$/e Å^{-3}	0.930/−0.487
Multipole refinement	
No. data in refinement	33162
No. refined parameters	973
GOF (F)	1.52
N_{ref}/N_r	34.0822
Final R_1 [$I > 3\sigma(I)$] (all data)	0.0271 (0.0667)
wR_2 [$I > 3\sigma(I)$]	0.0198
$\Delta\rho_{max/min}$/e Å^{-3}	0.437/−0.477

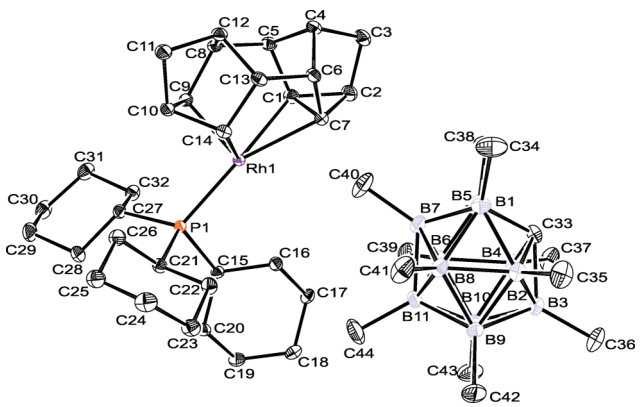

Fig. 2 ORTEP drawing of **[1–Cy][HCB$_{11}$Me$_{11}$]**, with ellipsoids depicted at 50% probability level. Hydrogen atoms omitted for clarity.

There is nothing remarkable about the C–C bonding in the cyclohexyl fragments of the tricyclohexylphosphine fragment. The topological properties at the C–C bcps in the fragment have values of $\rho(\boldsymbol{r})$ ranging from 1.58 to 1.71 e Å^{-3} and $\nabla^2\rho(\boldsymbol{r})$ varying between −7.69 to −10.58 e Å^{-5} which are consistent with the bonds being covalent. This, combined with C–C bond lengths of ~1.53 Å and ellipticity (ε) values of 0.00–0.08 indicate that the bonds are single. In a similar manner the topological parameters for the P–C bonds were consistent with them being single, covalent bonds

Table 2 Topological properties at the bond critical points for the $[Rh(C_{14}H_{16})(PCy_3)]^+$ cation in **[1–Cy][HCB$_{11}$Me$_{11}$]**

Bond	d_{ij}/Å	R_{ij}[a]/Å	$\rho(\mathbf{r}_{bcp})$/e Å^{-3}	$\nabla^2\rho(\mathbf{r}_{bcp})$/e Å^{-5}	$H(\rho)$/a.u.	$G(\rho)$/a.u.	$V(\rho)$/a.u.	ε
Rh1–C1	2.3649(6)	2.4391	0.42(1)	4.02(1)	–0.013	0.055	–0.068	8.33
Rh1–C7	2.3622(6)	—	—	—	—	—	—	—
Rh1–C9	2.0433(5)	2.0436	0.79(1)	6.25(2)	–0.056	0.124	–0.180	0.09
Rh1–C14	2.0403(5)	2.0405	0.80(1)	6.04(2)	–0.056	0.124	–0.180	0.09
Rh1–P1	2.2604(1)	2.2623	0.75(1)	3.56(1)	–0.056	0.096	–0.151	0.07
P1–C15	1.8631(4)	1.8640	1.16(2)	–5.62(3)	–0.167	0.108	–0.275	0.03
P1–C21	1.8498(5)	1.8501	1.22(2)	–6.39(3)	–0.181	0.115	–0.296	0.13
P1–C27	1.8474(5)	1.8483	1.19(2)	–6.26(3)	–0.176	0.111	–0.287	0.09
C1–C2	1.5145(9)	1.5150	1.63(2)	–5.98(5)	–0.288	0.228	–0.517	0.80
C1–C5	1.5348(8)	1.5350	1.62(2)	–8.41(5)	–0.294	0.208	–0.502	0.02
C1–C7	1.6101(9)	1.6150	1.34(2)	–0.25(4)	–0.194	0.193	–0.387	2.10
C2–C3	1.5179(10)	1.5182	1.72(3)	–10.50(5)	–0.326	0.219	–0.545	0.11
C2–C7	1.5147(9)	1.5162	1.60(2)	–5.65(5)	–0.277	0.220	–0.498	0.70
C3–C4	1.5299(9)	1.5300	1.66(2)	–9.20(5)	–0.307	0.214	–0.521	0.06
C4–C5	1.5535(9)	1.5536	1.58(2)	–7.93(4)	–0.280	0.200	–0.480	0.03
C4–C6	1.5504(8)	1.5507	1.56(2)	–7.56(4)	–0.273	0.197	–0.470	0.04
C5–C8	1.5455(8)	1.5458	1.62(2)	–9.49(4)	–0.297	0.201	–0.498	0.04
C6–C7	1.5341(8)	1.5342	1.70(2)	–9.56(5)	–0.318	0.220	–0.538	0.02
C6–C13	1.5512(8)	1.5513	1.60(2)	–8.77(4)	–0.289	0.200	–0.489	0.06
C8–C9	1.5594(8)	1.5598	1.63(2)	–7.77(4)	–0.293	0.213	–0.506	0.03
C8–C12	1.5484(8)	1.5489	1.58(2)	–7.57(4)	–0.280	0.203	–0.483	0.03
C9–C10	1.5381(8)	1.5385	1.62(2)	–8.26(4)	–0.293	0.209	–0.501	0.09
C10–C11	1.5267(8)	1.5275	1.67(2)	–9.62(5)	–0.310	0.212	–0.522	0.04
C10–C14	1.5435(7)	1.5442	1.63(2)	–8.10(4)	–0.293	0.211	–0.505	0.09
C11–C12	1.5252(8)	1.5255	1.68(2)	–8.65(5)	–0.307	0.219	–0.526	0.03
C12–C13	1.5508(8)	1.5509	1.61(2)	–7.56(4)	–0.288	0.211	–0.499	0.03
C13–C14	1.5604(8)	1.5606	1.55(2)	–7.63(4)	–0.272	0.195	–0.467	0.02
C15–C16	1.5462(6)	1.5463	1.60(1)	–8.11(2)	–0.285	0.203	–0.489	0.00
C15–C20	1.5367(6)	1.5368	1.61(1)	–8.66(2)	–0.292	0.204	–0.496	0.04
C16–C17	1.5302(6)	1.5303	1.64(1)	–9.32(2)	–0.302	0.207	–0.509	0.06
C17–C18	1.5256(7)	1.5260	1.68(1)	–10.18(3)	–0.315	0.212	–0.527	0.08
C18–C19	1.5301(8)	1.5303	1.71(1)	–10.47(2)	–0.324	0.218	–0.541	0.03
C19–C20	1.5339(7)	1.5341	1.63(1)	–9.17(2)	–0.299	0.206	–0.504	0.03
C21–C22	1.5406(7)	1.5406	1.61(1)	–8.49(2)	–0.289	0.203	–0.492	0.05
C21–C26	1.5429(7)	1.5432	1.58(1)	–7.69(2)	–0.279	0.201	–0.479	0.03
C22–C23	1.5287(7)	1.5288	1.65(1)	–9.41(2)	–0.303	0.208	–0.511	0.05
C23–C24	1.5293(8)	1.5293	1.71(1)	–10.58(3)	–0.326	0.218	–0.544	0.03
C24–C25	1.5326(9)	1.5326	1.66(1)	–9.90(2)	–0.310	0.209	–0.519	0.03
C25–C26	1.5316(7)	1.5316	1.64(1)	–9.28(2)	–0.301	0.207	–0.507	0.02
C27–C28	1.5367(7)	1.5367	1.61(1)	–8.63(2)	–0.292	0.205	–0.497	0.04
C27–C32	1.5404(7)	1.5405	1.61(1)	–8.37(2)	–0.290	0.205	–0.495	0.02
C28–C29	1.5379(7)	1.5379	1.63(1)	–9.25(2)	–0.299	0.206	–0.505	0.04
C29–C30	1.5338(10)	1.5338	1.67(1)	–10.10(3)	–0.317	0.214	–0.531	0.06
C30–C31	1.5257(9)	1.5262	1.67(1)	–9.98(2)	–0.311	0.209	–0.520	0.02
C31–C32	1.5314(7)	1.5315	1.65(1)	–9.45(2)	–0.305	0.209	–0.514	0.03
Rh1–H16A	2.3014(1)	2.3290	0.19(1)	2.11(1)	–0.0001	0.022	–0.022	0.24

[a] R_{ij} is the length of the bond path between atoms.

[$\rho(\mathbf{r}) = 1.16$–1.22 e Å^{-3}, $\nabla^2\rho(\mathbf{r}) = -5.62$ to -6.39 e Å^{-5}, $\varepsilon = 0.03$–0.13], see Table 2.

The scattering from the core electrons of heavy atoms dominates that from the valence electrons and as a result bcps are often located in regions of charge depletion [positive values of $\nabla^2\rho(\mathbf{r})$] or they are even missing where chemical intuition would expect them to be present.[16] As a result, when examining the bonding around rhodium it is necessary to consider the energetics at the bcps and not simply the signs and magnitudes of $\rho(\mathbf{r})$ and $\nabla^2\rho(\mathbf{r})$. Several schemes have been suggested to characterise such interactions around heavy atoms that are based on the total energy density [$H(\rho)$], the kinetic energy density [$G(\rho)$] and the potential energy density [$V(\rho)$].[17] Shared shell interactions have negative values of $H(\rho)$ and $|V(\rho)| > G(\rho)$, while the opposite is true for closed shell interactions which have positive values of $H(\rho)$ and $|V(\rho)| < G(\rho)$.[18] In general, more negative values of $H(\rho)$ tend to indicate a greater shared shell (covalent) nature to the interaction. In the case of the Rh1–P1 bcp, the associated topological values of $\rho(\mathbf{r})$ [0.75(1) e Å^{-3}] and $\nabla^2\rho(\mathbf{r})$ [3.56(1) e Å^{-5}] are more consistent with closed shell interactions, however the negative values of $H(\rho)$ [–0.056 a.u.] and $|V(\rho)| > G(\rho)$ both indicate some degree of covalency to the interaction. The assertion of some covalent character to the bond is supported by a plot of the Laplacian of $\rho(\mathbf{r})$ in the plane Rh1–P1–C1, which shows a clear charge concentration at P1 directed towards rhodium, see Fig. 3. In addition, a plot of the deformation density in the same plane shows clear evidence of electron density from phosphorus directed towards rhodium, see Fig. 4. It is worth noting that these topological values associated with the Rh1–P1 are in good agreement with those seen in our studies of the precursor complexes $Rh(C_7H_8)(PR_3)Cl$

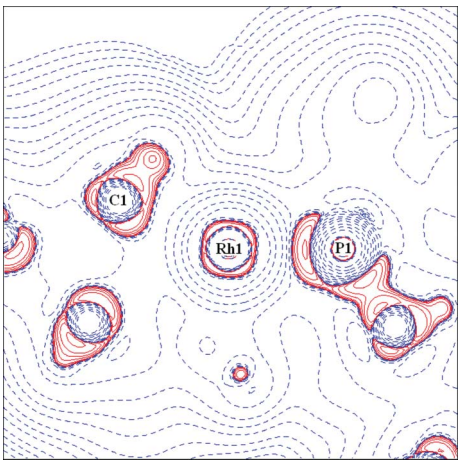

Fig. 3 Negative Laplacian of the electron density for **[1–Cy][HCB$_{11}$Me$_{11}$]**, in the plane of Rh1–P1–C1, positive contours are solid red lines, negative contours are dashed blue lines.

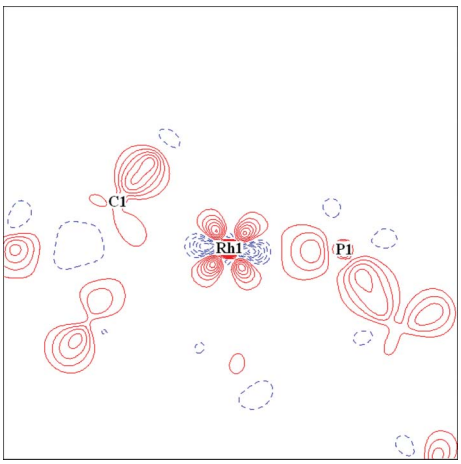

Fig. 4 Deformation density map for **[1–Cy][HCB$_{11}$Me$_{11}$]** in the plane of Rh1–P1–C1 after the multipole refinement. Contours are depicted at the 0.1 e Å^{-3} level, with positive contours as solid red lines and negative contours as dashed blue lines. The zero line is omitted.

(R = PPh$_3$, P^{t}Bu$_3$ and PCy$_3$). For example in Rh(C$_7$H$_8$)(PCy$_3$)Cl the topological parameters associated with the Rh1–P1 bond were $\rho(\boldsymbol{r}) = 0.64(1)$ e Å^{-3}, $\nabla^2\rho(\boldsymbol{r}) = 4.86(1)$ e Å^{-5}, $\varepsilon = 0.13$, $H(\rho) = -0.043$ a.u., $V(\rho) = -0.134$ a.u., $G(\rho) = 0.091$ a.u. and $|V(\rho)|/G(\rho) = 1.470$.

The C–C bonds in the Binor-S cage are all expected to be single, covalent bonds; examining Table 2, however it can be seen that there are three bonds (C1–C2, C1–C7 and C2–C7) for which the topological parameters are out of line with those seen for all other C–C bonds [$\rho(\boldsymbol{r})$ = 1.55–1.72 e Å^{-3}, $\nabla^2\rho(\boldsymbol{r})$ = −7.56 to −10.50 e Å^{-5}, ε = 0.02–0.11]. The remaining three bonds (C1–C2, C1–C7 and C2–C7) form a cyclopropane ring at the edge of the cage where the σ-interaction Rh1 ⋯ (C1–C7) is anticipated. The topological parameters associated with the two shorter sides (C1–C2 and C2–C7) of the three-membered ring, *i.e.* not directly interacting with Rh have very similar parameters, only slightly different from other C–C bonds in the cage, with $\rho(\boldsymbol{r}) \sim 1.61$ e Å^{-3} and $\nabla^2\rho(\boldsymbol{r}) \sim -5.8$ e Å^{-5}, while the C1–C7 bond has considerably lower values for both $\rho(\boldsymbol{r})$ [1.34(2) e Å^{-3}] and $\nabla^2\rho(\boldsymbol{r})$ [−0.25(4) e Å^{-5}]. These values suggest that all three C–C bonds are shared shell in nature, with the lower values of $\rho(\boldsymbol{r})$ and $\nabla^2\rho(\boldsymbol{r})$ for the C1–C7 bond showing that it has less electron density in the bond and it is therefore weaker than the other cage C–C bonds. This is supported by the energy related parameters at the bcps for which $H(\rho)$ is negative and $|V(\rho)| > G(\rho)$ in all three cases suggesting that the interactions have some degree of covalency. The [λ_1, λ_2, λ_3] eigenvalues associated with the C–C bonds are C1–C2 [−11.46, −6.38, 11.86], C2–C7 [−10.85, −6.39, 11.58] and C1–C7 [−8.54, −2.76, 11.05], and the comparatively small values of λ_2 indicate that the electron density is flatter in one direction perpendicular to the bond path than the other, particularly for C1–C7.

Three bond critical points were identified between rhodium and the C1, C9 and C14 carbon atoms of the Binor-S cage, no bond critical point was located between rhodium and C7. Overall the small positive values of $\rho(\boldsymbol{r})$ and $\nabla^2\rho(\boldsymbol{r})$, combined with a negative $H(\rho)$ and $|V(\rho)| > G(\rho)$, show some shared shell character to all three Rh–C interactions. Dealing first with the bcps relating to the carbon atoms (C9 and C14) that are not involved in the potential Rh ⋯ (C–C) σ-interaction, it can be seen that their topological parameters are very similar to each other [$\rho(\boldsymbol{r})$ ~0.80 e Å^{-3}, $\nabla^2\rho(\boldsymbol{r})$ ~6.1 e Å^{-5}, ε ~0.09 and $H(\rho) \sim -0.06$ a.u.]. At the other end of the cage (Rh1–C1) the smaller magnitudes of the values of $\rho(\boldsymbol{r})$ [0.42 (1) e Å^{-3}], $\nabla^2\rho(\boldsymbol{r})$ [4.02(1) e Å^{-5}] and $H(\rho)$ −0.013 a.u. indicate that the interaction is weaker than those to C9 and C14 despite still containing some degree of covalency [$|V(\rho)| > G(\rho)$]. Fig. 5 clearly supports this assertion with much larger charge concentration at C9 and C14 than C1, and similarly more evidence of electron density between Rh1 and the C9/C14 atoms compared to C1. It is worth noting at this point that this would have been expected, firstly because the Rh1–C9/C14 bond lengths are ~0.32 Å shorter than the Rh1–C1 bond length and secondly there is evidence of bonding between C1 and C7 in addition to bonding to two other carbon atoms, a hydrogen and rhodium as seen for C9 and C14.

The geometry of the Rh ⋯ (C–C) interaction would be expected to depend on whether it was ionic or covalent in nature. If it were purely ionic, a T-shaped interaction geometry would be expected with a bcp between the two carbon atoms and one between the metal and the C–C bcp. However, some degree of covalency would result in a ring structure with one C–C bcp, two Rh–C bcps and a ring critical point (rcp) at the centre of the three-membered ring, with the concave curvature of the bond paths decreasing as the covalency of the interaction increases.[19] The interpretation of "T"-shaped and "Y"-shaped bond paths in silver-alkyne complexes has been discussed and debated by Scherer *et al.*[20] and Krapp *et al.*[21] However, it is not uncommon for bond and ring critical points to coalesce in what is termed a bond catastrophe,[22] in the vicinity of heavy atoms due to small errors in the measured structure factors. Hence while all the expected bond and ring critical points (rcp) can be recovered from 'error free' theoretical electron densities this is often not the case for experimental data. For example in a charge density study on a Co dimer with alkene fragments bound to the metal centre the authors found the electron density to be very flat in the region of the Co–C═C triangles and only small changes in the electron density caused a bond catastrophe to occur.[23] In our experimental studies on the precursor species Rh(C$_7$H$_8$)(PR$_3$)Cl (R = PPh$_3$, P^{t}Bu$_3$ and PCy$_3$) we also observed flat electron density in the region of the Rh–C═C triangles and the occurrence of

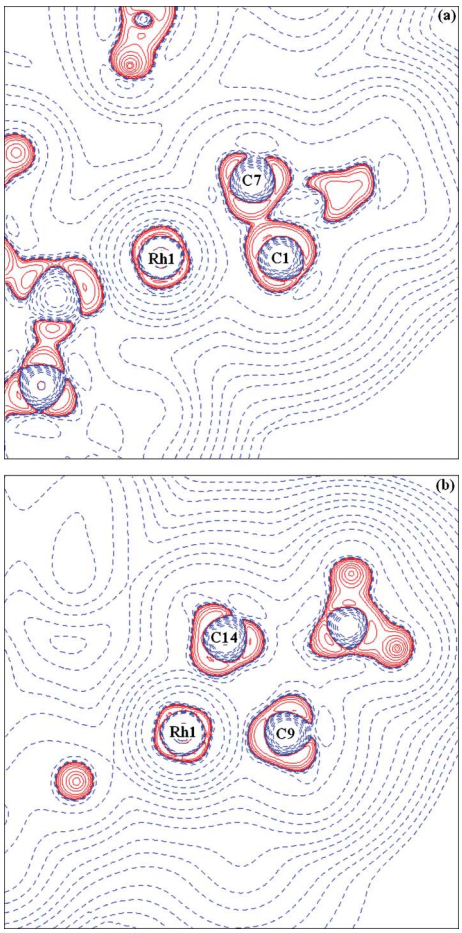

Fig. 5 Negative Laplacian of the electron density for **[1–Cy][HCB$_{11}$Me$_{11}$]**. Positive contours are solid red lines, negative contours are dashed blue lines. Drawn in the plane (a) Rh1–C1–C7, (b) Rh1–C9–C14.

bond catastrophes in all three cases. It was also noteworthy that the Rh–C bond paths were curved (endocyclic) and significantly longer than the separation of the atoms.[15] Given these points it is worth looking more closely at the nature of the Rh1 ··· C1–C7 interaction.

Only one Rh–C bcp (Rh1–C1) associated with the Rh1 ··· (C1–C7) σ-interaction was identified despite the fact that the separation of the atoms is essentially the same for Rh1–C1 and Rh1–C7 [Rh1–C1 2.3649(6) Å, Rh1–C7 2.3622(6) Å]. However, the elongation of the C1–C7 bond [1.6101(9) Å] compared to the remaining C–C bonds in the structure (~1.51–1.56 Å) and the equivalent bond in a derivative of free parent Binor-S (1.497(6) Å),[24] gives an indication of the activation of the C1–C7 bond. The ellipticity values at the two observed bcps for Rh1–C1 and C1–C7 are very high, at 8.33 and 2.10, respectively, indicating that the electron density is very flat in one direction perpendicular to the bond path. Hence small changes in the electron density appear to have resulted in a bcp and rcp coalescing in a bond catastrophe. In addition, the bond path (R_{ij}) for the Rh1–C1 interaction is significantly longer than the separation of the atoms (d_{ij}), in other words the bond path is curved in an endocyclic (concave) manner as illustrated in Fig. 6. The highly curved nature of the Rh1–C1 bond path suggests that while the interaction has some shared shell character it is not strongly covalent which would have resulted in a triangular

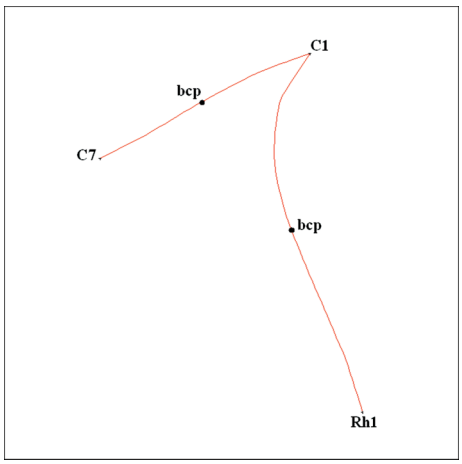

Fig. 6 Illustration of the bond paths in **[1–Cy][HCB$_{11}$Me$_{11}$]** between rhodium and C1–C7 of the Binor-S cage.

interaction geometry and a straight line for the M–C bond paths. This assertion is supported by the small negative value of $H(\rho)$ [–0.013 a.u.] and the fact that $|V(\rho)| > G(\rho)$ at the Rh1–C1 bcp, since as mentioned earlier the more negative the value of $H(\rho)$ and greater values of $|V(\rho)|$ compared to $G(\rho)$ the greater the covalency of the interaction. Examining the Laplacian of ρ shows a distortion of the charge concentrations associated with the C1–C7 bond towards the rhodium metal centre, Fig. 5a. In addition there is a small charge concentration at both C1 and C7 on the side of rhodium, which suggests the presence of an interaction between Rh1 and C1/C7. Carbon atoms which are not involved in an interaction to the metal centre would be expected to have a charge depletion directed towards the metal centre.[12b] Normal C–C single bonds not involved in a σ-interaction would be expected to have ellipticity profiles similar to than seen for C21–C22 in Fig. 7a. As mentioned earlier the presence of a σ C–C→Ti interaction caused a distortion in the ellipticity profile along the C–C bond paths of the titanacyclobutane ring on the Cα side of the C–C bcp.[11] Inspecting the ellipticity profile along the C1–C7 bond of the metallocyclopropane ring, where both carbon atoms would be expected to be equally involved in the σ-interaction, shows that the highest ellipticity is at the centre of the C–C bond path which supports the presence of an interaction (see Fig. 7b). In summary, the evidence suggests that there is a weak Rh1 ··· (C1–C7) σ-interaction in **[1–Cy][HCB$_{11}$Me$_{11}$]**, which has some degree of covalency associated with it. Given this, a ring structure would have been expected with three bcps and one rcp, however the Rh1–C7 bcp and consequently the rcp are missing. It is likely that the missing bcp is a result of a bond catastrophe having occurred on the basis of the flat electron density between Rh1 and C1–C7.

In order to gain further insights into the nature of the interactions between the rhodium metal centre and the norbornadiene fragment a theoretical study was also undertaken. A comparison of the experimental and theoretically derived topological properties is provided in Table 4. The topological parameters for the experimentally obtained Rh1–C interactions show reasonable agreement with the theoretical results although the values of $\nabla^2\rho(\boldsymbol{r})$ and $G(\rho)$ at Rh1–C9/14 bcps are smaller in the calculations. As found experimentally the topological parameters suggest that there is some shared shell character to the Rh1–C interactions.

Table 3 Topological properties at the bond critical points for the $[B_{11}C_{12}H_{34}]^-$ anion in $[Rh(C_{14}H_{16})(PCy_3)][B_{11}C_{12}H_{34}]$, **[1–Cy][HCB$_{11}Me_{11}$]**

Bond	d_{ij}/Å	R_{ij}[a]/Å	$\rho(\mathbf{r}_{bcp})$/e Å^{-3}	$\nabla^2\rho(\mathbf{r}_{bcp})$/e Å^{-5}	$H(\rho)$/a.u.	$G(\rho)$/a.u.	$V(\rho)$/a.u.	ε
C33–B1	1.7093(8)	1.7110	0.92(1)	–3.84(3)	–0.116	0.078	–0.194	2.57
C33–B2	1.7125(9)	1.7143	0.93(1)	–3.98(1)	–0.118	0.078	–0.196	2.61
C33–B3	1.7113(8)	1.7154	0.90(1)	–3.06(1)	–0.109	0.079	–0.187	2.70
C33–B4	1.7032(8)	1.7054	0.92(1)	–4.07(1)	–0.117	0.077	–0.194	2.48
C33–B5	1.7175(8)	1.7196	0.91(1)	–3.51(1)	–0.113	0.079	–0.192	2.70
C34–B1	1.5903(8)	1.5904	1.21(1)	–8.81(5)	–0.186	0.106	–0.291	0.07
C35–B2	1.5923(8)	1.5925	1.19(1)	–9.36(5)	–0.183	0.097	–0.280	0.04
C36–B3	1.5962(7)	1.5964	1.20(1)	–9.11(5)	–0.185	0.102	–0.288	0.08
C37–B4	1.5960(8)	1.5963	1.18(1)	–9.55(5)	–0.183	0.095	–0.278	0.09
C38–B5	1.5948(8)	1.5949	1.20(1)	–9.10(5)	–0.186	0.103	–0.289	0.09
C39–B6	1.6001(8)	1.6002	1.15(1)	–8.19(4)	–0.172	0.097	–0.270	0.04
C40–B7	1.6014(7)	1.6020	1.13(1)	–9.19(4)	–0.171	0.086	–0.257	0.03
C41–B8	1.5963(8)	1.5965	1.15(1)	–7.98(4)	–0.172	0.099	–0.272	0.12
C42–B9	1.5972(8)	1.5976	1.13(1)	–9.02(4)	–0.172	0.088	–0.260	0.06
C43–B10	1.5981(8)	1.5986	1.15(1)	–8.03(4)	–0.172	0.099	–0.271	0.07
C44–B11	1.5952(9)	1.5954	1.18(1)	–7.29(1)	–0.176	0.110	–0.287	0.07
B1–B2	1.7917(8)	1.7946	0.80(1)	–1.58(1)	–0.086	0.071	–0.157	5.77
B1–B5	1.7902(8)	1.7943	0.80(1)	–1.62(1)	–0.086	0.071	–0.157	4.97
B1–B7	1.7823(8)	1.7831	0.83(1)	–2.25(1)	–0.094	0.072	–0.168	2.62
B1–B8	1.7818(8)	1.7832	0.82(1)	–2.20(1)	–0.093	0.072	–0.166	2.96
B2–B3	1.7887(8)	1.7918	0.81(1)	–1.63(1)	–0.087	0.071	–0.158	5.35
B2–B8	1.7789(8)	1.7796	0.84(1)	–2.30(1)	–0.095	0.072	–0.167	2.58
B2–B9	1.7803(8)	1.7817	0.83(1)	–2.23(1)	–0.092	0.070	–0.162	2.94
B3–B4	1.7928(7)	1.7982	0.81(1)	–1.62(1)	–0.086	0.070	–0.156	4.50
B3–B9	1.7768(8)	1.7777	0.84(1)	–2.34(1)	–0.096	0.072	–0.168	2.61
B3–B10	1.7817(8)	1.7828	0.83(1)	–2.20(1)	–0.092	0.070	–0.162	2.94
B4–B5	1.7963(7)	1.7980	0.81(1)	–1.46(1)	–0.085	0.071	–0.164	6.63
B4–B6	1.7781(7)	1.7807	0.83(1)	–2.17(1)	–0.093	0.071	–0.164	3.01
B4–B10	1.7768(8)	1.7775	0.84(1)	–2.34(1)	–0.096	0.073	–0.169	2.69
B5–B6	1.7749(8)	1.7750	0.86(1)	–2.67(1)	–0.099	0.072	–0.171	2.13
B5–B7	1.7793(8)	1.7808	0.83(1)	–2.23(1)	–0.092	0.070	–0.162	2.94
B6–B7	1.7957(8)	1.7985	0.81(1)	–1.86(1)	–0.087	0.069	–0.156	3.22
B6–B10	1.7916(7)	1.7978	0.81(1)	–2.09(1)	–0.088	0.068	–0.156	3.11
B6–B11	1.7923(8)	1.7957	0.82(2)	–2.18(1)	–0.089	0.067	–0.156	2.47
B7–B8	1.7954(8)	1.7975	0.82(1)	–2.14(1)	–0.089	0.068	–0.157	2.68
B7–B11	1.7892(8)	1.7900	0.80(1)	–1.77(1)	–0.087	0.069	–0.155	3.75
B8–B9	1.7973(8)	1.7983	0.82(1)	–2.12(1)	–0.089	0.068	–0.156	2.54
B8–B11	1.7902(9)	1.7953	0.81(2)	–1.94(1)	–0.087	0.068	–0.155	2.88
B9–B10	1.7987(8)	1.8001	0.82(1)	–2.12(1)	–0.089	0.068	–0.157	2.67
B9–B11	1.7938(7)	1.7962	0.79(2)	–1.80(1)	–0.084	0.066	–0.151	3.44
B10–B11	1.7887(8)	1.7917	0.79(2)	–1.79(1)	–0.086	0.068	–0.153	3.23

[a] R_{ij} is the length of the bond path between atoms.

Table 4 Comparison of selected topological properties at the bond critical points for the $[Rh(C_{14}H_{16})(PCy_3)]^+$ cation in **[1–Cy][HCB$_{11}$Me$_{11}$]**; (top) experimental, (bottom, italics) calculated[a]

Bond	d_{ij}/Å	$\rho(\mathbf{r}_{bcp})$/e Å^{-3}	$\nabla^2\rho(\mathbf{r}_{bcp})$/e Å^{-5}	$H(\rho)$/a.u.	$G(\rho)$/a.u.	$V(\rho)$/a.u.	ε
Rh1–C1	2.3649(6)	0.42(1)	4.02(1)	–0.013	0.055	–0.068	8.33
	2.387	*0.37*	*3.92*	*–0.008*	*0.049*	*–0.057*	*0.91*
Rh1–C7	2.3622(6)	—	—	—	—	—	—
	2.391	*0.36*	*3.92*	*–0.008*	*0.049*	*–0.057*	*1.03*
Rh1–C9	2.0433(5)	0.79(1)	6.25(2)	–0.056	0.124	–0.180	0.09
	2.055	*0.81*	*2.97*	*–0.045*	*0.076*	*–0.121*	*0.02*
Rh1–C14	2.0403(5)	0.80(1)	6.04(2)	–0.056	0.124	–0.180	0.09
	2.057	*0.81*	*2.94*	*–0.044*	*0.075*	*–0.120*	*0.03*
C1–C7	1.6101(9)	1.34(2)	–0.25 (4)	–0.194	0.193	–0.387	2.10
	1.623	*1.23*	*–3.79*	*–0.123*	*0.083*	*–0.206*	*1.25*
C21–C22	1.5406(7)	1.61(1)	–8.49(2)	–0.289	0.203	–0.492	0.05
	1.545	*1.57*	*–12.63*	*–0.188*	*0.057*	*–0.188*	*0.01*
Rh1–H16A	2.3014(1)	0.19(1)	2.11	–0.0001	0.022	–0.022	0.24
	2.389	*0.15*	*1.41*	*–0.002*	*0.017*	*–0.019*	*0.64*
Rh–C1–C7 ccp[a]		*0.36*	*4.17*				

[a] ccp = Cage critical point (calculated values only).

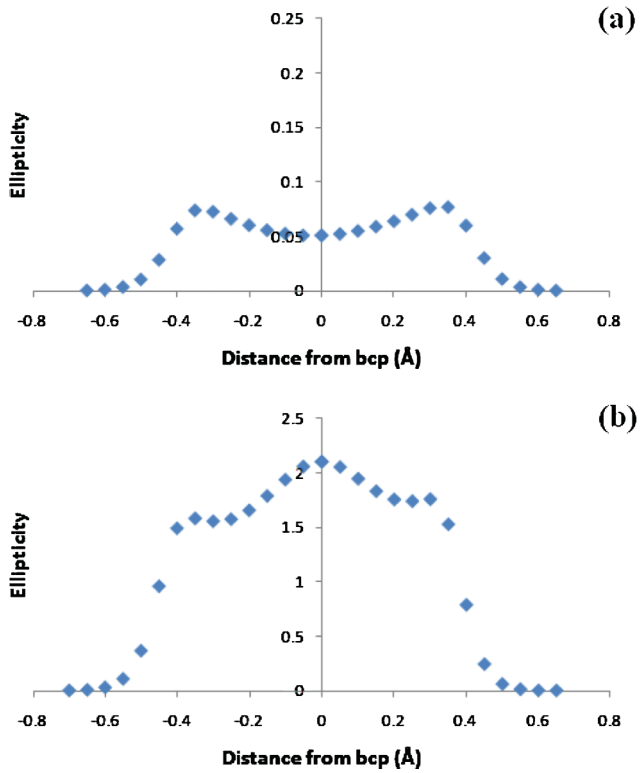

Fig. 7 Ellipticity profile in **[1–Cy][HCB$_{11}$Me$_{11}$]** along the (a) C21–C22 bond path, (b) C1–C7 bond path.

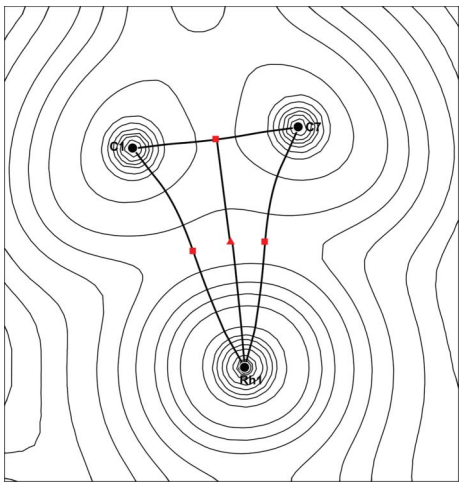

Fig. 8 Illustration of the calculated electron density, critical points and bond paths for the Rh–C1–C7 interaction in **[1–Cy][HCB$_{11}$Me$_{11}$]**. Red squares denote bond critical points and the red triangle a ring critical points.

There are also small differences between the experimental and theoretical topological parameters at the C1–C7 bcp, most notable in the larger theoretical value for $\nabla^2\rho(r)$, however both results clearly support the fact that it is a shared shell covalent interaction. The key difference between the results is that a bond catastrophe has not yet occurred in the theoretical calculation and all four Rh–C bcps were identified. This clearly shows the presence of a weak Rh1 $\cdots$ (C1–C7) σ-interaction. However, the high calculated ellipticities at the Rh1–C1/C7 and C1–C7 bcps do suggest that the electron density is flat in one direction perpendicular to the bond path. These facts combined with the values of the remaining topological parameters and the slightly endocyclically curved bond paths (Fig. 8), indicate that a small change in the electron density could result in a bond catastrophe occurring, which is in line with the experimental results.

C–H agostic interactions can be characterised experimentally in a number of ways including diffraction, NMR spectroscopy and vibrational spectroscopy. In terms of diffraction both X-ray, or more accurately for hydrogen atom positioning, neutron diffraction studies have been used to provide a geometrical basis (the C–H and M $\cdots$ H distance and M $\cdots$ H–C angle) to characterise an agostic interaction. Alternatively, NMR spectroscopy can provide insight into the presence of an agostic interaction where an upfield shift of the relevant ^{1}H NMR signal is observed.[1,3] In X-ray charge density work a number of studies have been undertaken to characterise the topological features associated with an agostic interaction.[12] These studies have noted distinct differences between the topological properties of α and β agostic interactions. Indeed it has been suggested that α agostic interactions should be more correctly described as α agostic geometry due to a lack of M $\cdots$ H bcp.[25] Moreover it has been noted that the computational approach used can affect whether an M $\cdots$ H bcp is recovered for β agostic interactions. It has been suggested that β agostic interactions in d^0 metal complexes are caused by negative hyperconjugative delocalisation of the M–C bonding electron density as opposed to (C–H)→M donation.[12c] Hence the closeness of the M and H is a consequence of the negative hyperconjugative rather than the presence of a direct M $\cdots$ H interaction. In the case of the d^0 metals it has been postulated that evidence for an agostic bond can be obtained from a distortion of the electron density along the C–C bond path towards the metal centre, thus resulting in an increased ellipticity for the C–C bond and an asymmetric ellipticity profile in a plane perpendicular to the C–C bond path. However, it has been noted that in less electropositive, later, transition-metal complexes, (C–H) $\cdots$ M donation does play a significant role.

NMR spectroscopy shows that the agostic C–H interaction in **[1-Cy]$^+$** is only weak at best, with no significant chemical shift change observed for those CH_2 groups implicated.[7] This is consistent with the solid-state structure that showed only a weak interaction [Rh $\cdots$ CH_3 2.901(3) Å]. In the charge density study herein, an interaction was identified between Rh1 and H(16A), the topological parameters of which indicate that it is a weak interaction on the border between an ionic and covalent interaction, with $\rho(r)$ = 0.19(1) e Å^{-3}, $\nabla^2\rho(r)$ = 2.11(1) e Å^{-5}, ε = 0.24, $H(\rho)$ = –0.0001 a.u. and $|V(\rho)| \approx G(\rho)$. Examining the deformation density shows a very small distortion of the electron density in the C16–H16A bond near H16A towards Rh, which is also apparent in a plot of the electron density, see Fig. 9 and 10. However, it was also noted that there was a small charge depletion in the Laplacian at C16 which was directed towards Rh in the plane Rh1–C16–H16A although this was not present in the plane Rh1–C15–C16, it suggests that C16 is not strongly interacting with Rh1, see Fig. 11. Due to the size and complexity of the structure, the C–H bond lengths in the structure were fixed at their expected neutron values, and hence it would be meaningless to examine the C–H bond length for elongation. However, it was

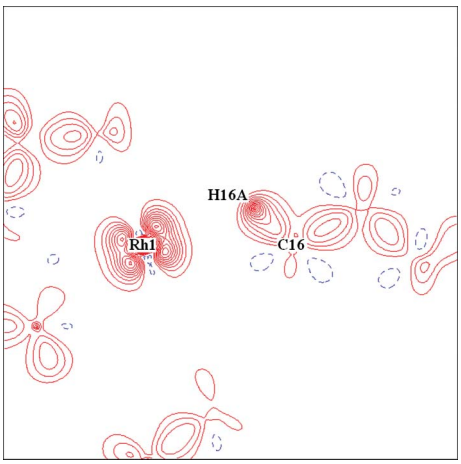

Fig. 9 Deformation density map for **[1–Cy][HCB$_{11}$Me$_{11}$]**, drawn in the plane of Rh1–C16–H16A. Contours are depicted at the 0.1 e Å^{-3} level. Positive contours are solid red lines, negative contours are dashed blue lines and the zero line is omitted.

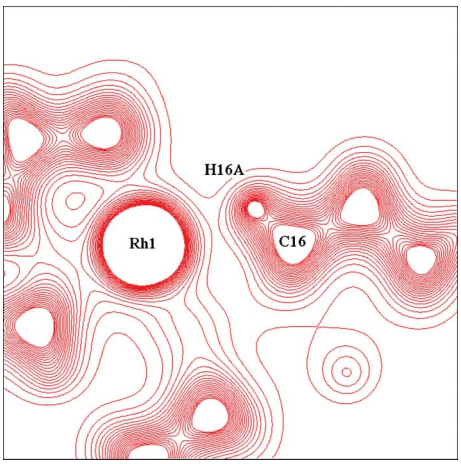

Fig. 10 The electron density in the Rh1–C16–H16A plane for **[1–Cy][HCB$_{11}$Me$_{11}$]**. Contours are depicted at the 0.1 e Å^{-3} level.

noted that the ε value of 0.01 at the C16–H16A bcp was in line with those of other C–H bonds in the structure, similarly the ε (0.02) at the C15–C16 bcp was consistent with that of other C–C bonds. In summary this suggests that there is a weak interaction between Rh1$\cdots$H16, although this γ-H interaction does not fit very well with the topological description established for a β-agostic bond in early transition metals. The lack of a significant agostic C–H interaction perhaps should come as no surprise, given its location *trans* to the alkyl ligands of the metallacyclobutane, as high *trans* influence ligands can result in vacant sites opposite that are not filled by agostic interactions.[26] The theoretical results support the presence of a weak interaction between Rh1$\cdots$H16 (Fig. 12), with good agreement between the experimental and theoretically derived topological parameters at the bcp, see Table 4.

By chance the $[B_{11}C_{12}H_{34}]^-$ anion is also of interest from a charge density perspective and so it is worth examining briefly the bonding within it. The topological properties associated with the $[B_{11}C_{12}H_{34}]^-$ anion are provided in Table 3. The carborane cage consists of 11 boron atoms and 1 carbon atom, with each cage atom bound to five other cage atoms and one terminal atom (in

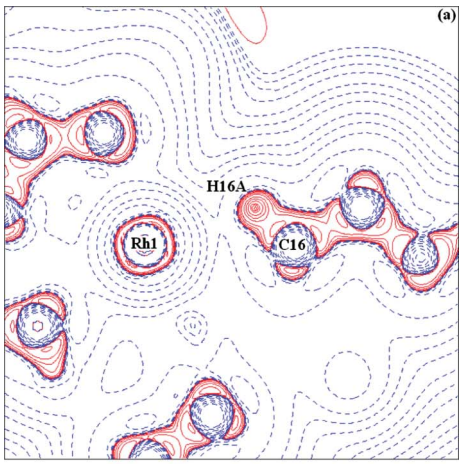

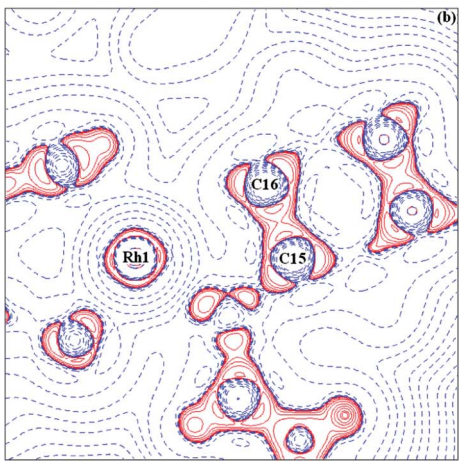

Fig. 11 Negative Laplacian of the electron density for **[1–Cy][HCB$_{11}$Me$_{11}$]**. Positive contours are solid red lines, negative contours are dashed blue lines. Drawn in the plane (a) Rh1–C16–H16A, (b) Rh1–C15–C16.

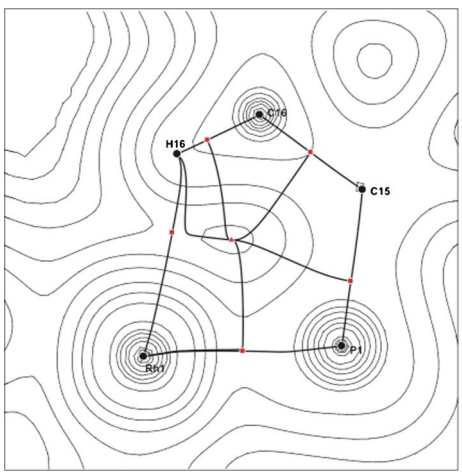

Fig. 12 Illustration of the calculated electron density, critical points and bond paths for the Rh–H16–C16–C15–P interaction in **[1–Cy][HCB$_{11}$Me$_{11}$]**. Red squares denote bond critical points and red triangle ring critical points.

the case of the boron atoms the terminal atom is a methyl carbon, while for the carbon the terminal atom is a hydrogen

atom). The anion contains two different types of B–C bonding involving the cage boron atoms, those to the exterior methyl carbon atoms and also bonds to C33 which forms part of the carborane cage. All of the B–C bonding was, as expected, classified as covalent on the basis of the topological properties at the B–C bcps and associated parameters. The B–$C_{terminal}$ bcps had $\rho(\boldsymbol{r})$ values ranging from 1.13 to 1.21 e Å^{-3}, negative values for $\nabla^2\rho(\boldsymbol{r})$ between –7.29 and –9.55 e Å^{-5} and ε of 0.03–0.11, while the bond lengths were all around 1.60 Å. The B–C33 bcps had $\rho(\boldsymbol{r})$ of 0.90–0.93 e Å^{-3} and $\nabla^2\rho(\boldsymbol{r})$ ranged between –3.06 and –4.07 e Å^{-5}. These values are considerably lower than the B–$C_{terminal}$ indicating that the B–C33 bonds are weaker, however this would be anticipated as C33 is bonding to five cage boron atoms and delocalisation of the electron density over the cage would be expected, while the other carbon atoms are only interacting with one boron atom. This is reflected in the B–C bond lengths, with the B–C33 bond lengths being ~0.11 Å longer than those for the B–$C_{terminal}$ bonds. The ellipticity values for B-C33 range from 2.48 to 2.70, due to the relatively small λ_2 values, indicating that the electron density is flat in one orientation perpendicular to the bonds; this is likely to be as a result of delocalisation of the electron density over the cage.

Moving on to examine the B–B bonding in the anion, it can be seen that the B–B bonds in which both the boron atoms (B1–B5) also bond to C33 have slightly different topological parameters to those boron atoms further down the cage, although all parameters indicate the bonds to be covalent. At the bcps for the bonds involving B1 to B5 bonding to each other, $\rho(\boldsymbol{r})$ is ~0.81 e Å^{-3}, with $\nabla^2\rho(\boldsymbol{r})$ of –1.46 to –1.63 e Å^{-5} and ε values of 4.50–6.63, while the remaining B–B bcps have $\rho(\boldsymbol{r})$ of 0.79–0.86 e Å^{-3}, $\nabla^2\rho(\boldsymbol{r})$ values between –1.77 and –2.34 e Å^{-5} and ε values of 2.13–3.75. Again the high ellipticities are due to electron delocalisation across the surface of the cage. Various plots of the Laplacian of $\rho(\boldsymbol{r})$ and the deformation density are provided in Fig. S3 and S4 in ESI†. A number of previous charge density studies have been carried out on boranes[27] and carboranes,[28,29] and the values of $\rho(\boldsymbol{r})$ and $\nabla^2\rho(\boldsymbol{r})$ associated with the cage B–B and B–C bonds in the current study are of similar magnitudes to those seen in other charge density studies on carboranes.[29,30] In a similar situation to that seen in other borane and carborane cages,[27,29] some of the bond paths associated with the bonds in the cage are curved, albeit in the current study only very slightly where the maximum difference seen in the bond path length and the separation of the atoms is ~0.01 Å.

Conclusion

The results presented here demonstrate a successful charge density analysis of $[Rh(C_{14}H_{16})(PCy_3)][B_{11}C_{12}H_{34}]$, **[1–Cy][HCB$_{11}Me_{11}$]**. It has provided a rare chance to examine both experimentally and theoretically the interactions around the rhodium metal centre, including a Rh $\cdots$ (C–C) σ-interaction, a putative intermediates in transition-metal activated C–C bond activation.

Two Rh $\cdots$ (C–C) interactions scenarios are possible depending on whether the interaction is purely ionic or contains some degree of covalency. In the former a T-shaped interaction geometry would be expected while the latter would give a more triangular interaction geometry. Only one Rh–C bcp was identified in **[1–Cy][HCB$_{11}$Me$_{11}$]**, despite the fact that the similar atomic separations for Rh1–C1 and Rh1–C7 indicated that both atoms may interact with rhodium. However, the distortion of the charge concentrations associated with the C1–C7 bond towards Rh1 in the Laplacian supports the assertion that both C1 and C7 interact with rhodium. Given that the electron density in the Rh1–C1–C7 triangle is very flat, it seems reasonable to suggest that a bond catastrophe has occurred explaining the missing Rh1–C7 bcp. The presence of a Rh1 $\cdots$ (C1–C7) σ-interaction was identified on the basis of the elongation of the C1–C7 bond and the ellipticity profile along the C1–C7 bond path, and classified as a weak covalent interaction on the basis of the topological properties at the Rh1–C1 bcp. The interaction showed a concave curvature of the Rh1–C1 bond path away from a T-shaped bond path scenario which would have been expected for an ionic interaction. The topological properties associated with the C1–C7 bond indicated that while the interaction was still covalent, it was considerably weaker than other C–C bonds in the structure, supporting the assertion that the bond had been activated. The theoretical calculations strongly supported the experimental results identifying the presence of a weak Rh1 $\cdots$ (C1–C7) σ-interaction. The calculations also illustrated that the electron density was very flat in the region of Rh1–C1–C7 meaning that only very small changes in the electron density would be required for the experimentally observed bond catastrophe to occur.

Additionally it was noted that the interactions in the $[B_{11}C_{12}H_{34}]^-$ anion were consistent with previous charge density studies on carborane cages.

Experimental

Synthesis

[1–Cy][HCB$_{11}$Me$_{11}$]. A solution of PCy_3 (9.6 mg, 0.034 mmol) in CH_2Cl_2 (2 mL) was added dropwise to a solution of $[Rh(nbd)_2][HCB_{11}Me_{11}]$ (20 mg, 0.034 mmol, prepared by addition of $Ag[HCB_{11}Me_{11}]$[14a] to $[Rh(nbd)Cl]_2$/excess nbd) in CH_2Cl_2 (2 mL) and the solution was stirred for 10 min. Pentane (10 mL) was added and the mixture was allowed to stand for 1 h. The precipitate was collected by filtration and dissolved in $C_6H_4F_2$. Slow diffusion of pentane into the resulting solution at 5 °C gave the product as yellow crystals (10 mg, 34%).

^{1}H-NMR (400 MHz, CD_2Cl_2): δ 3.26 (br 4H), 2.30 (m, 2H), 2.18 (m, 3H, PCH), 2.14 (s, 2H), 1.96 (s, 4H), 1.74–1.92 (m, 15H, cyclohexyl CH_2), 1.45–1.60 (m, 6H, cyclohexyl CH_2), 1.40 (s, 4H), 1.25–1.45 (m, 9H, cyclohexyl CH_2), 1.13 (s, BCH), –0.19 (s, 15H, CH_3), –0.44 (s, 15H, CH_3), –0.56 (s, 3H, CH_3).

^{31}P{^{1}H} NMR (162 MHz, CD_2Cl_2): δ 35.72 [d, J(RhP) 211 Hz]

X-Ray diffraction

A high-resolution X-ray diffraction dataset was recorded on a Nonius Kappa CCD diffractometer using graphite monochromated Mo-Kα radiation (λ = 0.71073 Å) at 100(2) K. The data were collected using the strategy calculated by the *COLLECT* software[31] and integrated using *HKL Scalepack*.[32] The data were subsequently merged and corrected for absorption using *SORTAV*[33] within the *WINGX* suite.[34] A total of 484435 measured reflections were merged to give 46189 unique reflections which had an R_{int} of 5.56%; there were two missing reflections up to

$\sin\theta/\lambda = 1.06$ Å^{-1}. The structure was solved using direct methods in *SHELXS*[35] and refined by full-matrix least squares on F^2 in *SHELXL-97*.[35]

The spherical atom model was subsequently used as the starting point for a multipole refinement within XD2006,[36] which implements the multipole formalism of Hansen and Coppens.[37] In order to obtain the best refinement a number of different models were used and all of the available and appropriate databanks were tested, given the presence of a second-row transition metal (Rh) exclusion of relativistic effects can significantly affect the accuracy of the topological properties obtained from the refinement,[38] with this in mind STO–Dirac–Fock atomic relativistic wavefunctions[39] were used in the final refinement. The electronic configuration $5s^1 4d^8$ was used for rhodium with the $5s^1$ scattering contribution fixed as part of the core contribution. The anisotropic displacement parameters for the hydrogen atoms were estimated using the *SHADE2* web server[40] and fixed throughout the refinement. Initially only the scale factor was refined, followed by the non-hydrogen atomic positions and displacement parameters. Subsequently, a high-order refinement ($\sin\theta/\lambda > 0.7$ Å^{-1}) was carried out to determine the optimal atomic positions and displacement parameters for the non-hydrogen atoms. This was followed by a low-order refinement ($\sin\theta/\lambda < 0.7$ Å^{-1}) of the positional parameters of the H atoms. In all further refinement cycles, the C–H bond lengths were reset to their average neutron diffraction distances of 1.08 Å (methyl and ethyl) and 1.10 Å (non-ethyl cage H). The multipole expansion was truncated at the hexadecapole level for rhodium, phosphorus and chlorine, the octupole level for all carbon and boron atoms and the bond directed dipole level for the H atoms. Due to the large size of the complex the anion and the cation were put into two groups and the charges on the groups maintained throughout the refinement using the commands KEEP charge group 1, KEEP charge group 2 and KEEP charge group 3. Ten κ parameters were refined along with seven κ' parameters for the non-hydrogen atoms, the κ' parameters were constrained to be the same for all multipoles. At the end of the multipole refinement a plot of scale factor *vs*. resolution for the dataset was satisfactory with a maximum variation of $<\pm 3\%$ around unity, see Fig. S1 (ESI†). The residual density map at the end of the refinement using all data was almost featureless (HP = 0.44, DH = –0.48) and the Hirshfeld rigid bond test[41] was satisfactory, see Table S1 (ESI†). Further details of the data collection and refinement are provided in Table 1. The energy densities at the bond critical points, after completion of the multipole refinement, were derived using the Abramov approximation implemented in *WinXPRO*.[42]

Computational calculations

Geometry optimisation was carried out using the Amsterdam Density Functional package (version ADF2010.02).[43] The Slater-type orbital (STO) basis sets were of triple-ζ quality augmented with two polarization function (ADF basis TZ2P). Core electrons were frozen (C 1s; P 2p; Rh 3d) in our model of the electronic configuration for each atom (except H). Relativistic effects were included by virtue of the zero order regular approximation (ZORA).[44] The local density approximation (LDA) by Vosko, Wilk and Nusair (VWN)[45] was used together with the exchange correlation corrections of Becke[46] and Perdew[47] (BP86). A full geometry optimization was performed using X-ray parameters as a starting point. The optimized structural parameters from the ADF calculation were then used as input for a single point density functional calculation using Gaussian 09),[48] in order to generate a wavefunction (.wfn) file. The same approximations and corrections (LDA/VWN/BP86) were used as for the ADF calculation. The Gaussian-type orbital (GTO) basis sets were DGDZVP for Rh and TZVP for P, C and H.[49] Topological analyses of the electron density was performed using the AIM2000 program.[50]

Acknowledgements

The authors would like to thank the EPSRC (EP/E048994/1) for funding. The assistance of Professor Vladimir Tsirelson in modifying WinXPro to deal with the number of atoms in our structure is also gratefully acknowledged. H. A. S. would also like to thank the Leverhulme Trust and University of Durham for financial support.

References

1 G. J. Kubas, *Metal dihydrogen and σ-bond complexes*, Kluwer Academic/Plenum Publishers, New York, 2001.
2 G. J. Kubas, *Chem. Rev.*, 2007, **107**, 4152–4205.
3 M. Brookhart, M. L. H. Green and G. Parkin, *Proc. Natl. Acad. Sci. U. S. A.*, 2007, **104**, 6908–6914.
4 B. Rybtchinski and D. Milstein, *Angew. Chem., Int. Ed.*, 1999, **38**, 870–883.
5 For examples see: (*a*) A. Vigalok, B. Rybtchinski, L. J. W. Shimon, Y. Ben-David and D. Milstein, *Organometallics*, 1999, **18**, 895–905; (*b*) M. Gandelman, L. Konstantinovski, H. Rozenberg and D. Milstein, *Chem.–Eur. J.*, 2003, **9**, 2595–2602; (*c*) B. L. Madison, S. B. Thyme, S. Keene and B. S. Williams, *J. Am. Chem. Soc.*, 2007, **129**, 9538–9539; (*d*) C. Boulho, T. Keys, Y. Coppel, L. Vendier, M. Etienne, A. Locati, F. Bessac, F. Maseras, D. A. Pantazis and J. E. McGrady, *Organometallics*, 2009, **28**, 940–943.
6 Crystallographically isolated examples include: (*a*) R. Tomaszewski, I. Hyla-Kryspin, C. L. Mayne, A. M. Arif, R. Gleiter and R. D. Ernst, *J. Am. Chem. Soc.*, 1998, **120**, 2959–2960; (*b*) B. G. Harvey, C. L. Mayne, A. M. Arif, R. Tomaszewski and R. D. Ernst, *J. Am. Chem. Soc.*, 2006, **128**, 1770–1770; (*c*) J. Jaffart, M. L. Cole, M. Etienne, M. Reinhold, J. E. McGrady and F. Maseras, *Dalton Trans.*, 2003, 4057–4064; (*d*) J. Jaffart, M. Etienne, M. Reinhold, J. E. McGrady and F. Maseras, *Chem. Commun.*, 2003, 876–877; (*e*) O. T. Summerscales, F. G. N. Cloke, P. B. Hitchcock, J. C. Green and N. Hazari, *Science*, 2006, **311**, 829–831; (*f*) M. Etienne, J. E. McGrady and F. Maseras, *Coord. Chem. Rev.*, 2009, **253**, 635–646.
7 (*a*) S. K. Brayshaw, J. C. Green, G. Kociok-Kohn, E. L. Sceats and A. S. Weller, *Angew. Chem., Int. Ed.*, 2006, **45**, 452–456; (*b*) S. K. Brayshaw, E. L. Sceats, J. C. Green and A. S. Weller, *Proc. Natl. Acad. Sci. U. S. A.*, 2007, **104**, 6921–6926; (*c*) A. B. Chaplin, J. C. Green and A. S. Weller, *J. Am. Chem. Soc.*, 2011, **133**, 13162–13168.
8 C. H. Jun, *Chem. Soc. Rev.*, 2004, **33**, 610–618.
9 (*a*) R. A. Periana and R. G. Bergman, *J. Am. Chem. Soc.*, 1986, **108**, 7346–7355; (*b*) D. D. Wick, T. O. Northcutt, R. J. Lachicotte and W. D. Jones, *Organometallics*, 1998, **17**, 4484–4492; (*c*) M. E. Evans, T. Li and W. D. Jones, *J. Am. Chem. Soc.*, 2010, **132**, 16278–16284.
10 R. F. W. Bader and H. J. Essén, *J. Chem. Phys.*, 1984, **80**, 1943–1960.
11 S. Scheins, M. Messerschmidt, M. Gembicky, M. Pitak, A. Volkov, P. Coppens, B. G. Harvey, G. C. Turpin, A. M. Arif and R. D. Ernst, *J. Am. Chem. Soc.*, 2009, **131**, 6154–6160.
12 (*a*) P. L. A. Popelier and G. Logothetis, *J. Organomet. Chem.*, 1998, **555**, 101–111; (*b*) W. Scherer, P. Sirsch, D. Shorokhov, M. Tafipolsky, G. S. McGrady and E. Gullo, *Chem.–Eur. J.*, 2003, **9**, 6057–6070; (*c*) W. Scherer and G. S. McGrady, *Angew. Chem., Int. Ed.*, 2004, **43**, 1782–1806; (*d*) D. A. Pantazis, J. E. McGrady, M. Besora, F. Maseras and M. Etienne, *Organometallics*, 2008, **27**(6), 1128–1134; (*e*) S. Pillet, G. Wu, V. Kulsomphob, B. G. Harvey, R. D. Ernst and P. Coppens, *J. Am. Chem. Soc.*, 2003, **125**, 1937–1949.
13 S. Körbe, P. J. Schreiber and J. Michl, *Chem. Rev.*, 2006, **106**, 5208–5249.

14 (*a*) A. J. Clarke, M. J. Ingleson, N. J. Patmore, G. Kociok-Köhn, M. F. Mahon, G. D. Ruggiero, A. S. Weller and J. P. Rourke, *J. Am. Chem. Soc.*, 2004, **126**, 1503; (*b*) M. J. Ingleson, A. Clarke, M. F. Mahon, J. P. Rourke and A. S. Weller, *Chem. Commun.*, 2003, 1930.
15 (*a*) H. A. Sparkes, S. B. Brayshaw, A. S. Weller and J. A. K. Howard, *Acta Crystallogr., Sect. B: Struct. Sci.*, 2008, **64**, 550–557; (*b*) H. A. Sparkes, A. B. Chaplin, A. S. Weller and J. A. K. Howard, *Acta Crystallogr., Sect. B: Struct. Sci.*, 2010, **66**, 503–514.
16 L. J. Farrugia, C. Evans and M. Tegel, *J. Phys. Chem.*, 2006, **110**, 7952–7961.
17 D. Cremer and E. Kraka, *Angew. Chem., Int. Ed. Engl.*, 1984, **23**, 627–628.
18 (*a*) P. Macchi, D. M. Prosperpio and A. Sironi, *J. Am. Chem. Soc.*, 1998, **120**, 13429–13435; (*b*) J. Overgaard, I Turrel and D. E. Hibbs, *Dalton Trans.*, 2007, 2171–2178; (*c*) L. J. Farrugia, C. Evans, D. Lentz and M. Roemer, *J. Am. Chem. Soc.*, 2009, **131**, 1251–1268.
19 P. Macchi, D. M. Proserpio and A. Sironi, *J. Am. Chem. Soc.*, 1998, **120**, 1447–1455.
20 (*a*) A. Reisinger, N. Trapp, I. Krossing, S. Altmannshofer, V. Herz, M. Presnitz and W. Scherer, *Angew. Chem., Int. Ed.*, 2007, **46**, 8295–8298; (*b*) D. Himmel, N. Trapp, I. Krossing, S. Altmannshofer, V. Herz, G. Eickerling and W. Scherer, *Angew. Chem., Int. Ed.*, 2008, **47**, 7798–7801.
21 A. Krapp and G. Frenking, *Angew. Chem., Int. Ed.*, 2008, **47**, 7796–7797.
22 R. F. W. Bader, *Atoms in Molecules, A Quantum Theory*, Oxford University Press, 1990.
23 (*a*) J. Overgaard, H. F. Clausen, J. A. Platts and B. B. Iversen, *J. Am. Chem. Soc.*, 2008, **130**, 3834–3843; (*b*) J. Overgaard, J. A. Platts and B. B. Iversen, *Acta Crystallogr., Sect. B: Struct. Sci.*, 2009, **65**, 715–723.
24 L. D. Accolti, C. Fusco, G. B. Lucchini, G. B. Carpenter and R. Curci, *J. Org. Chem.*, 2001, **66**, 9063–9066.
25 I. Vidal, S. Melchor, I Alkorta, J. Elguero, M. R. Sundberg and J. A. Dobado, *Organometallics*, 2006, **25**(23), 5638–5647.
26 H. Braunschweig, K. Radacki and K. Uttinger, *Chem.–Eur. J.*, 2008, **14**, 7858–7866.
27 D. Förster, S. Scheins, P. Luger, D. Lentz and W. Preetz, *Eur. J. Inorg. Chem.*, 2007, 3169–3172.
28 I. V. Glukhov, Lyssenko, K. A. Korlyukov, A. A. Antipin and M. Yu, *Faraday Discuss.*, 2007, **135**, 203–215.
29 K. A. Lyssenko, M Yu. Antipin and V. N. Lebedev, *Inorg. Chem.*, 1998, **37**, 5834–5843.
30 M. Antipin, R. Boese, D. Bläser and A. Maulitz, *J. Am. Chem. Soc.*, 1997, **119**, 326–333.
31 Nonius, *COLLECT*, Nonius BV, Delft, The Netherlands, 1999.
32 Z. Otwinowski and W. Minor, *Methods Enzymol.*, 1997, **276**, 307–326.
33 R. H. Blessing, *J. Appl. Crystallogr.*, 1997, **30**, 421–426.
34 L. J. Farrugia, *J. Appl. Crystallogr.*, 1999, **32**, 837–838.
35 G. M. Sheldrick, *Acta Crystallogr., Sect. A: Found. Crystallogr.*, 2008, **64**, 112–122.
36 A. Volkov, P. Macchi, L. J. Farrugia, C. Gatti, P. Mallinson, T. Richter and T. Koritsanszky, *XD2006, a computer program package for multipole refinement and topological analysis of charge densities from diffraction data*, 2006.
37 N. K. Hansen and P. Coppens, *Acta Crystallogr., Sect. A: Cryst. Phys., Diffr., Theor. Gen. Crystallogr.*, 1978, **34**, 909–921.
38 G. Eickerling, R. Mastalerz, V. Herz, W. Scherer, H-J. Himmel and M. Reiher, *J. Chem. Theory Comput.*, 2007, **3**, 2182–2197.
39 (*a*) P. Macchi and P. Coppens, *Acta Crystallogr., Sect. A: Found. Crystallogr.*, 2001, **57**, 656–662; (*b*) Z. Su and P. Coppens, *Acta Crystallogr., Sect. A: Found. Crystallogr.*, 1998, **54**, 646–652.
40 A. O. Madsen, *J. Appl. Crystallogr.*, 2006, **39**, 757–758.
41 F. L. Hirshfeld, *Acta Crystallogr., Sect. A: Cryst. Phys., Diffr., Theor. Gen. Crystallogr.*, 1976, **32**, 239–244.
42 A. Stash and V. Tsirelson, *J. Appl. Crystallogr.*, 2002, **35**, 371–373.
43 (*a*) E. J. Baerends, D. E. Ellis and P. Ros, *Chem. Phys.*, 1973, **2**, 41–51; (*b*) L. Versluis and T. Ziegler, *J. Chem. Phys.*, 1988, **88**, 322–328; (*c*) G te Velde and E. J. Baerends, *J. Comput. Phys.*, 1992, **99**, 84–98; (*d*) C. F. Guerra, J. G. Snijders, G. te Velde and E. J. Baerends, *Theor. Chem. Acc.*, 1998, **99**, 391–403.
44 (*a*) J. G. Snijders, E. J. Baerends and P. Ros, *Mol. Phys.*, 1979, **38**, 1909–1929; (*b*) T. Ziegler, V. Tschinke, E. J. Baerends, J. G Snijders and W. J. Ravenek, *J. Phys. Chem.*, 1989, **93**, 3050–3056; (*c*) E van Lenthe, E. J. Baerends and J. G. Snijders, *J. Chem. Phys.*, 1993, **99**, 4597–4610.
45 S. H. Vosko, L. Wilk and M. Nusair, *Can. J. Phys.*, 1980, **58**, 1200–1211.
46 A. D. Becke, *Phys. Rev. A: At., Mol., Opt. Phys.*, 1988, **38**, 3098–3100.
47 J. P. Perdew, *Phys. Rev. B*, 1986, **33**, 8822–8824.
48 M. J. Frisch, G. W. Trucks, H. B. Schlegel, G. E. Scuseria, M. A. Robb, J. R. Cheeseman, J. Montgomery, J. A. T. Vreven, K. N. Kudin, J. C. Burant, J. M. Millam, S. S. Iyengar, J. Tomasi, V. Barone, B. Mennucci, M. Cossi, G. Scalmani, N. Rega, G. A. Petersson, H. Nakatsuji, M. Hada, M. Ehara, K. Toyota, R. Fukuda, J. Hasegawa, M. Ishida, T. Nakajima, Y. Honda, O. Kitao, H. Nakai, M. Klene, X. Li, J. E. Knox, H. P. Hratchian, J. B. Cross, V. Bakken, C. Adamo, J. Jaramillo, R. Gomperts, R. E. Stratmann, O. Yazyev, A. J. Austin, R. Cammi, C. Pomelli, J. W. Ochterski, P. Y. Ayala, K. Morokuma, G. A. Voth, P. Salvador, J. J. Dannenberg, V. G. Zakrzewski, S. Dapprich, A. D. Daniels, M. C. Strain, O. Farkas, D. K. Malick, A. D. Rabuck, K. Raghavachari, J. B. Foresman, J. V. Ortiz, Q. Cui, A. G. Baboul, S. Clifford, J. Cioslowski, B. B. Stefanov, G. Liu, A. Liashenko, P. Piskorz, I. Komaromi, R. L. Martin, D. J. Fox, T. Keith, M. A. Al-Laham, C. Y. Peng, A. Nanayakkara, M. Challacombe, P. M. W. Gill, B. Johnson, W. Chen, M. W. Wong, C. Gonzalez and J. A. Pople, Gaussian Inc., Pittsburgh, PA, 2009.
49 (*a*) N. Godbout, D. R. Salahub, J. Andzelm and E. Wimmer, *Can. J. Chem.*, 1992, **70**, 560–571; (*b*) C. Sosa, J. Andzelm, B. C. Elkin, E. Wimmer, K. D. Dobbs and D. A. Dixon, *J. Phys. Chem.*, 1992, **96**, 6630–6636.
50 (*a*) http://www.aim2000.de/; (*b*) F Biegler-König, J. Schönbohm and D. Bayles, AIM2000 - A Program to Analyze and Visualize Atoms in Molecules, *J. Comput. Chem.*, 2001, **22**, 545–559; (*c*) F. Biegler-König and J. Schönbohm, An Update to the AIM2000 - Program for Atoms in Molecules, *J. Comput. Chem.*, 2002.

